Computers and Concrete, Vol. 7, No. 1 (2010) 39-51
DOI: http://dx.doi.org/10.12989/cac.2010.7.1.039

Simulation of brittle fracture of autoclaved aerated concrete

I. Kadashevich

Otto-von-Guericke-Universität Magdeburg, Institut für Experimentelle Physik, Leipziger Str. 44, 39120 Magdeburg, Germany

D. Stoyan†

TU Bergakademie Freiberg, Institut für Stochastik, 09596 Freiberg, Germany

(Received December 17, 2007, Accepted July 17, 2009)

Abstract The system of pores of autoclaved aerated concrete (AAC) is described by the so-called cherry-pit model, a random system of partially interpenetrating spheres. For the simulation of fracture processes, the solid phase is approximated by an irregular spatial network of beams obtained by means of the so-called radical tessellation with respect to the pore spheres. FE calculations using standard software (ANSYS) yield the strain energies of the beams. These energies are used as fracture criterion according to which highly loaded beams are considered as broken and are removed from the network. The paper investigates the relationship between mean fracture strength and microstructure for structures close to real AAC samples and virtual structures with particular geometrical properties.

Keywords: porous material; spherical pores; fracture strength; equivalent network; FE simulation; strain energy.

1. Introduction

The prediction of mean fracture strength of porous materials using microstructural information is a difficult problem (e.g., Bazant and Planas 1997, Krajcinovic 1996, Sahimi 2003, Nishida 2004, Böhm 2004). It depends obviously on the microstructure of the material, in particular on porosity as the most important structural parameter. In more detail the microstructure can be described by means of stochastic models (e.g., Torquato 2002) or numerical data obtained by digital imaging methods such as microtomography or magnetic resonance imaging. Based on such data macroscopic, mechanical properties of materials such as Young modulus have been obtained by numerical calculations, usually by FE simulations. The classical way uses a discretisation of the solid phase by means of many polyhedral volume elements, which are usually much smaller than the pores (e.g., Stroeven and Stroeven 2001, and Stroeven *et al.* 2004). A successful approach of this type is the digital-image-based FE method of Garboczi (1998) and Garboczi and Day (1995), where the porous medium (for example a closed-cell cellular solid) is approximated by a system of cubic voxels. Ryan & van Rietbergen (2005) approximated the solid phase of bones by systems of small quadratic columns and used then 8-noded brick elements in FE calculations. Another approach uses lattice models or networks of one-dimensional mechanical elements. It dates back to Hrennikoff (1941)

† Corresponding author, E-mail: stoyan@math.tu-freiberg.de

and was later used, e.g., in Lin and Cohen (1982), Sahimi and Arabi (1993a,b), Pothuaud *et al.* (2000), Roberts *et al.* (2002) and Lachihab and Sab (2005). Krajcinovic (1996) emphasized the value of networks in micromechanics in general.

The mentioned papers differ in the construction of the network and in the manner in which neighbouring network elements interact. A successful approach in the use of Delaunay meshes as introduced by Christ *et al.* (1982), see also Okabe *et al.* (2000). There the network is given by a Voronoi tessellation and the one-dimensional elements are given by the dual Delaunay tessellation. The Voronoi tessellation may be constructed using irregular points in the material as in Bolander and Sukumar (2005) or may be closer adapted to the geometrical structure of the material (Lachihab and Sab 2005, and Kadashevich and Stoyan, 2005, 2008).

In the context of analyses of mechanical properties of AAC, in Kadashevich and Stoyan (2005, 2008) a beam network or framework was constructed that approximates the solid phase of AAC, based on a stochastic-geometric structure model according to which the pores are spherical and partially interpenetrating. The corresponding solid phase is approximated by a system of cylindrical irregularly arranged beams of spatially variable geometry, using the so-called radical tessellation. This is a natural generalisation of the better known Voronoi tessellation, see Gervois *et al.* (2002), Richard *et al.* (2001) and Telley *et al.* (1996). It assigns to a system of hard spheres a system of convex polyhedra, where each polyhedron contains just one sphere. The beams result from the edges of polyhedra and have lengths comparable with the pore diameters.

The present paper uses the same approach as Kadashevich and Stoyan (2008) for the analysis of fracture strength. The beam model constructed is incrementally loaded and the strain energies of the deformed beams are observed. Beams with a strain energy H_i above a suitably chosen level h_{crit} are considered as broken and are eliminated. The corresponding stress-displacement curve is recorded and fracture of the whole network is assumed to occur at that load where the first local maximum of the stress-strain curve is reached. This approach is first used to reproduce results of real fracture experiments with AAC in order to demonstrate the accuracy and applicability of the beam model approach. Encouraged by the good coincidence of experiments and model calculations, some virtual AACs are analysed which are based on variation of some important structure model parameters. This leads to interesting statements on the influence of microstruture on fracture strength of AAC.

2. Modeling the pore system and equivalent networks

In order to make the paper self-contained, the geometrical structure model used for the system of pores is briefly explained; for details see Kadashevich and Stoyan (2008) and Kadashevich et al. (2005). It is assumed that the pores are interpenetrating spheres, and the whole system of pores is fitted by the cherry-pit model or penetrable-concentric-shell model (Torquato 2002), which is a successful model also for other materials than AAC. Note that in the given AAC context the term 'pores' is applied to so-called macro pores or artificial pores, which have diameters between 25 μm and 1 mm. The corresponding porosity is called 'artificial porosity'.

In the model, each sphere consists of a hard non-interpenetrating spherical pit (or kernel) and a soft spherical shell. The system of pits is a random system of hard spheres of variable diameters. In the present paper, such systems are non-equilibrium packed systems of spheres, simulated by means of the force-biased algorithm, see Bezrukov *et al.* (2002) and Illian *et al.* (2008). Given the system of pits, the cherry-pit structure can be easily generated. The radius of the whole i^{th} sphere is R_i,

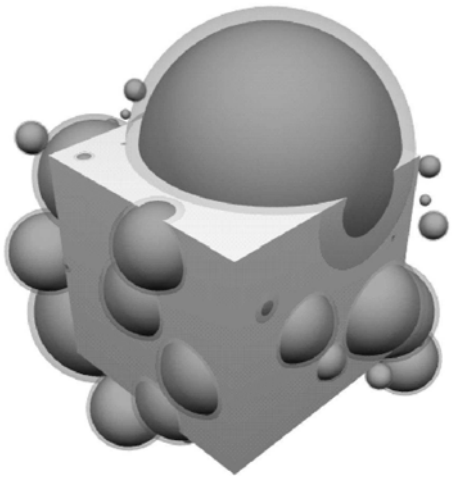

Fig. 1 A fragment of a cherry-pit model. The partly interpenetrating spheres have a hard pit (in black) and a soft shell (in light grey)

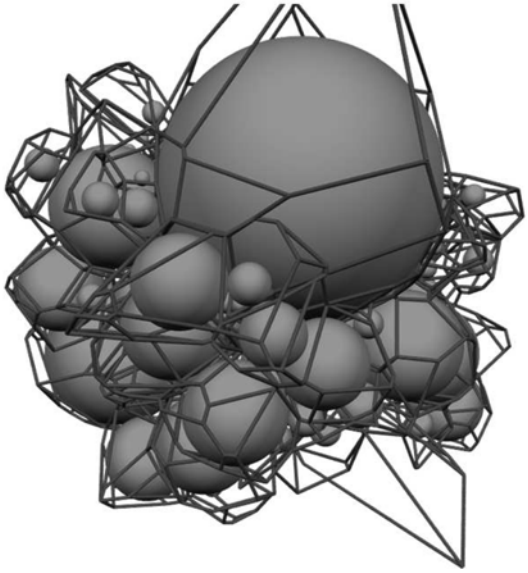

Fig. 2 A fragment of a radical tessellation, constructed for the pits in Fig. 1. Still some of the edges go through the soft parts of the spheres and will therefore removed in the construction of the final framework

while that of its pits is r_i, with $r_i = \lambda R_i$ with some fixed λ, $0 < \lambda \leq 1$, called cherry-pit factor. The case $\lambda = 1$ corresponds to the hard sphere case; in the present paper λ is between 0.9 and 1. See Fig. 1 for a visualization.

Given the cherry-pit structure, the solid phase is replaced by a system of cylindrical beams, which form a spatial network or frame work. The topology of the network and the geometrical parameters of its beams are obtained by means of a spatial tessellation, namely the radical tessellation (or Laguerre, weighted Voronoi, or power tessellation), see Gervois *et al.* (2002), Richard *et al.* (2001) and Telley *et al*. (1996). It is constructed with respect to the system of kernels and the result is then such that all tessellation cells are convex polyhedra and each contains one kernel. The following inequality gives the mathematical definition of the radical tessellation cell corresponding to the *i*th sphere with centre P_i and radius r_i: All points P satisfying

$$d^2(P_i,P) - r_i^2 \leq d^2(P_j,P) - r_j^2 \quad \text{for all spheres with centre } P_j \text{ and radius } r_j \ (j \neq i)$$

form this cell, where $d(P,Q)$ is the Euclidean distance of the points P and Q. For constructing Laguerre tessellations in the present paper Luc Oger's (Gervois *et al.* 2002) program is used.

The edges of the cells serve as axes of cylindrical beams and their lengths are the cylinder heights. The cylinder radii are constructed according to the neighbourhoods of the edges as described in the following. Edges going through soft shells (in terms of the porous structure they go through pore space) are removed as well as isolated edges (not connected with the general network). Only the remaining edges are used to construct the cylindrical beams. The radius ρ_k of the cylinder around the k^{th} edge is taken as the minimum of two distances: maximum distance of this edge to the

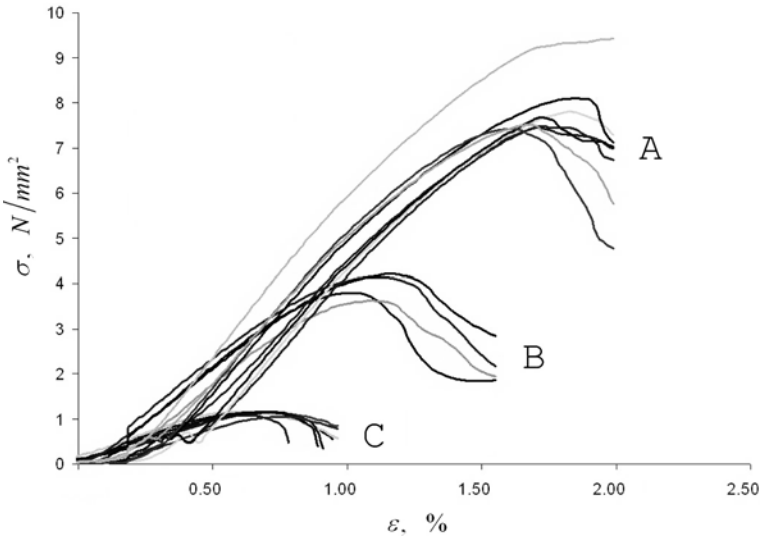

Fig. 3 Stress-strain curves for the samples A, B and C, σ= stress, ε= strain

surfaces of the spheres in the (usually three) cells that share this edge and minimum distance between the k^{th} edge and all other edges from neighbour cells not in direct contact with that edge. Fig. 3 tries to give an impression of the final beam structure.

3. Experiments

The investigations of the present paper are based on real AAC samples. They were produced in the laboratory of the Institute of Ceramics, Glass and Construction Materials of TU Bergakademie Freiberg by Dr. H.J. Schneider. Table 1 shows the main macroscopic material parameters for three samples, called types A – C. These types were produced under identical conditions; the structural differences, in particular the different porosities, result from quantity or type of powdered aluminium as pore agent; see Kadashevich *et al.* (2005) for more details.

From all four types test cubes of side length 55 mm were taken. Their orientation in the concrete blocks followed the direction of expansion, which is considered as the vertical direction. The cubes were cut out with a precision machine with a diamond cut-of wheel and then the specimens were wet-ground so that the sides became flat and parallel, with a tolerance of less than 0.1 mm on 100 mm. Finally, the cubes were dried at 50°C until mass constancy.

The samples were mechanically tested under uniaxial compression in vertical direction using a

Table 1 Macroscopic material parameters of the AAC samples

Types	Bulk density d, g/cm^3	Artificial porosity P_{Air}, %	Total porosity P, %	Capillary porosity $P_{Capillary}$, %
A	0.814	16.6	69.1	47.4
B	0.485	53.0	81.6	26.7
C	0.535	44.0	79.7	31.9

Table 2 Macroscopic mechanical parameters of the AAC samples

Samples	Young modulus E, N/mm^2	Fracture stress $\overline{\sigma}$, N/mm^2
A	695	7.61
B	346	3.79
C	389	1.14

standard material testing machine. For each material type 30-50 stress-controlled tests according to DIN EN 679 were carried out with constant loading rate 0.1 MPa/sec. The samples were placed unsupported in the testing machine, the results were recorded digitally with the help of testing machine software (TIRAtest).

The ultimate load was determined as the first maximum of the measured stress-strain curve. The fracture stress was calculated as the ultimate load divided by the cross-sectional area of the sample. Fig. 3 shows some stress-strain curves for the types A – C. The macroscopic Young moduli and mean fracture stresses obtained from the experiments are presented in Table 2.

The experimental results for the AAC samples follow essentially classical relationships for porous materials. In particular, the well-known relationship between Young modulus E and porosity P (e.g., Gibson and Ashby 1997) is satisfied in good approximation. However, E is also influenced by other structure properties, in particular by the degree of inhomogeneity.

For the mechanical calculations, the beams are assigned linear elastic isotropic material properties with identical Young modulus E_{beam} and Poisson ratio ν_{beam} in the whole network. Nevertheless, because of dierent beam diameters and lengths the mechanical behaviour of beams differs. The numerical values of these parameters $E_{beam}=13.540$ N/mm^2 and $\nu_{beam}=0.2$ were found as described in Kadashevich and Stoyan (2008). The latter is the usual value for concrete, while the Young modulus was determined experimentally and fortunately turned out to be the same for all AAC types.

4. Finite element simulation for elasticity modulus

The equivalent networks constructed as described in section 2 were used in Kadashevich and Stoyan (2008) in order to investigate the relationship between microstructure and macroscopic Young modulus E. The calculations were carried out with ANSYS v.8 with BEAM44 elements, which are 3D beams with 6 degrees of freedom in each node and cylindrical cross-section. The mechanical load situation in the FE calculations follows the experiments carried out as shown in Fig. 5.

The networks have free boundary conditions on the side surfaces if they are large enough (larger than the representative volume element) and symmetrical boundary conditions for smaller samples. The edge ends are fixed in the loading direction on bottom and top and prescribed displacements are applied at the edges.

The summary strain in the numerical simulations was chosen as 1.5%, which is similar to the situation in the laboratory tests for the AAC samples, where the maximum strain was 2%. Therefore problems with contacts between edges in the network can be neglected.

In Kadashevich and Stoyan (2007) also the size of representative volume element (RVE) was

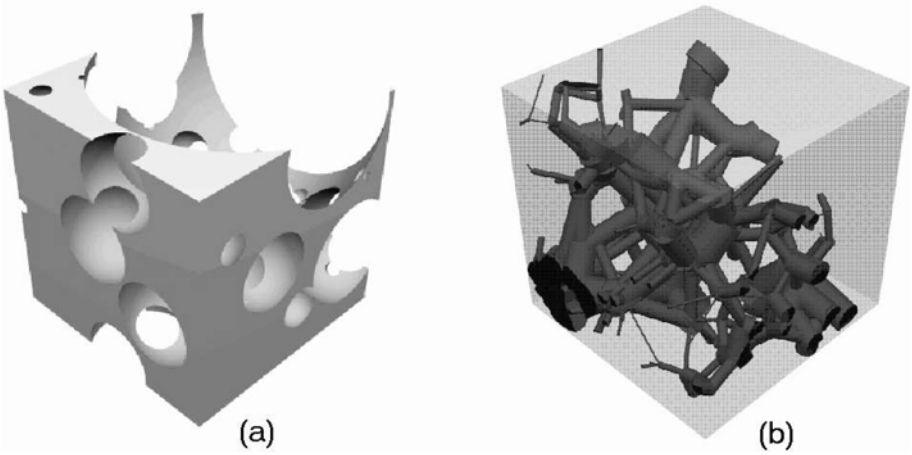

Fig. 4 A fragment of a porous medium according to the cherry-pit model. (a) The solid phase corresponding to the pores of Fig. 1; (b) the beams that replace the solid phase in (a)

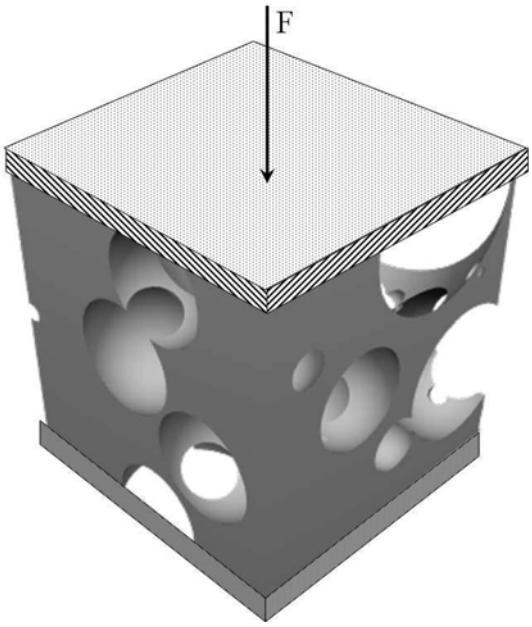

Fig. 5 Loading scheme for the FE analysis of AAC samples

investigated. The RVE is the minimum dimension of a cube containing an equivalent network that yields the same macroscopic mechanical parameter (in the given case: E) as very large (infinite) cubes. It turned out that the RVEs, if measured in mm, depend of AAC type. However, if they are measured by number of beams, a nearly unique value was obtained: For all AAC samples a value of 40,000 beams was obtained, which corresponds e.g., to a cube side length of 6.5 mm for AAC type A. These RVEs are rather large in comparison to RVEs given in the literature for similar materials.

5. Finite element simulation of fracture

This section demonstrates that also fracture processes can be modelled by means of the beam model approach. This provides an effective framework for the study of fracture behaviour of porous materials on computers and to avoid expensive experiments. In particular, the influence of the microstructure on fracture behaviour can be studied systematically, based on systematically varied computer-generated virtual material samples, and furthermore materials until now not existing can be tested.

The fracture simulation aims to reproduce loading histories such as presented in Fig. 4. This is realized by the model approach described in the preceding sections, but now made time-dependent, with increasing load. Again equivalent networks are used and FE calculations.

In order to simulate the nonlinear fracture process, the total deformation is approximated as a series of small linear steps, and for each of these steps the linear elastic problem is solved by means of ANSYS. This is supported by external subroutines that prepare the network for the next loading

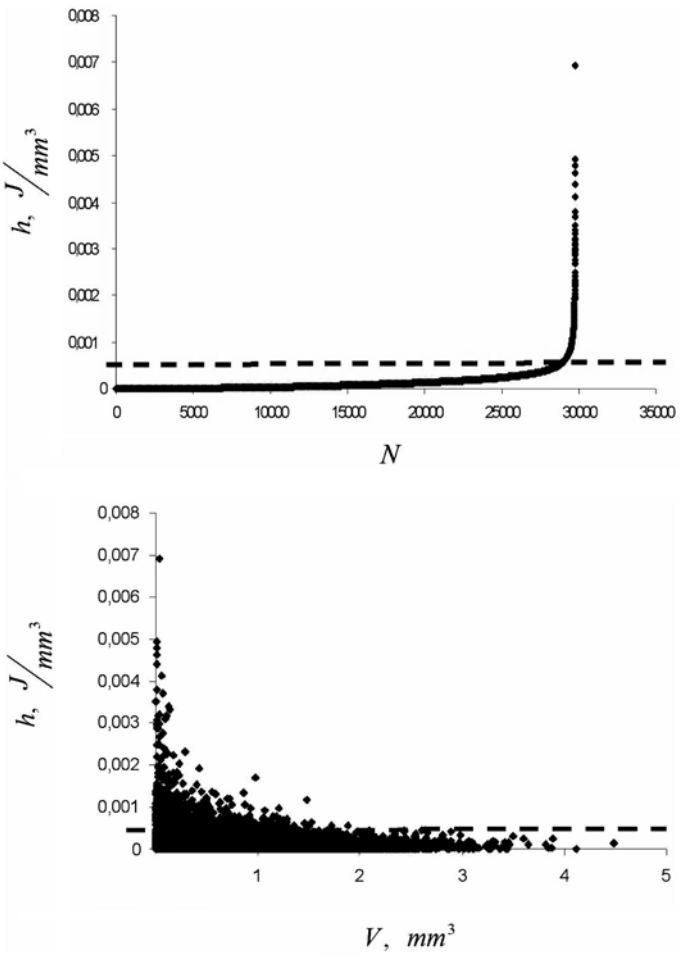

Fig. 6 Distribution of strain energy h in the beams in a loaded network without removed beams. Frequency distribution of strain energy (above), relationship between beam volume and strain energy (below). ⋯ = critical strain level h_{crit}

step and remove overloaded (broken) beams. The reader should note that in the case of the strain-controlled scheme described in Section 4 the total elastic energy of the system may be not conserved. Removing of broken beams simulates dissipation of energy used for fracture. Fig. 7 below shows that our approach yields correct results.

The procedure of removing beams is based on the local strain energy for every beam. Under increasing load, in the network strain energy is accumulated, which depends for every beam on the individual displacements of its nodal sites. These energies or beam strains are considered as responsible for beam fractures. If the first beam energies exceed a given level, the corresponding beams break and are removed from the network. The remaining network is loaded further, and again the most loaded beams break etc.

The fracture criterion used here deviates a little from the usual criterion using the fracture energy release rate G_f as in Bazant and Planas (1997), which uses energy divided by cross section area of beam. The reason is that in the networks considered here the beams can have lengths of the same order as their diameters, such that it cannot be guaranteed that fractures go through the cross-sections. Therefore, also the beam lengths must be considered. Therefore the fracture criterion for the beams is chosen so that the beam energies are related to beam volume.

That means, weighted energies are used, given by

$$h = \frac{H}{V} \tag{1}$$

where H is the strain energy of the loaded beam and V its volume. The critical strain level h_{crit} was taken as h_{crit}=0.0005 J/mm^3 . This value results from numerical experiments with different values of critical strain levels as that which yielded the best approximation of the experimental data. As Fig. 6 shows for a typical case, this value is exceeded only by a very small number of beams.

Fig. 7 shows results of calculations of this kind: stress-displacement diagrams for simulated samples of a structure similar to type A, where the prescribed displacement is 20 μm. Additionally, Fig. 8 presents the number of beams excluded from the system in dependence of load. Statistical analysis showed that the whole samples break if 8-10% of the beams are broken.

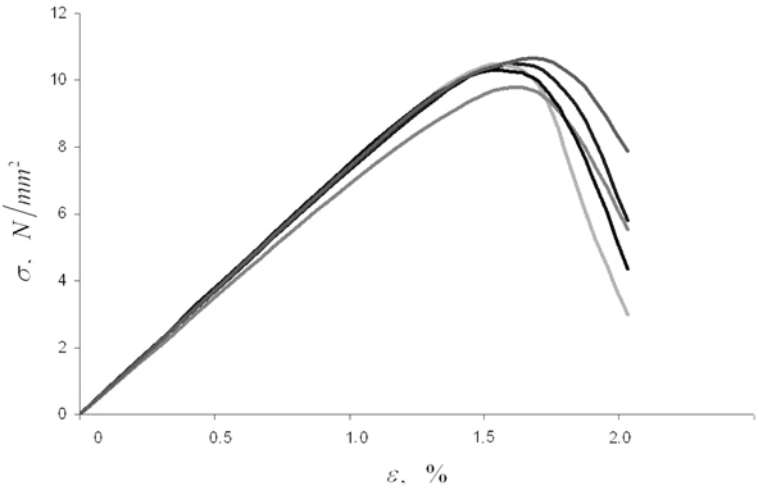

Fig. 7 Stress-strain curves for simulated samples of type A with loading increment 20 μm

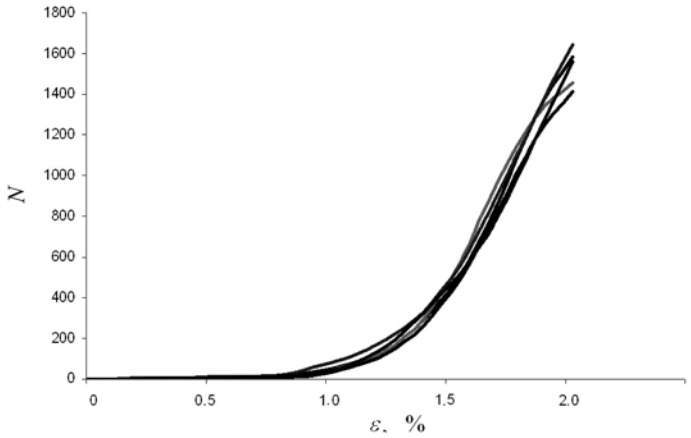

Fig. 8 Number of beams suffering fracture under increasing load for the processes of Fig. 7. The total number of beams in the beginning is 50.000

Table 3 Experimental and calculated mean fracture strength $\overline{\sigma}$ for the AAC samples

Samples Calculated	Artificial porosity $\overline{\sigma}$, N/mm^2	Experimental $\overline{\sigma}$, N/mm^2
A	8.14	10.31
B	3.92	5.35
C	1.16	1.05

The relationship to AAC is given by the beam parameters E=13, 540 N/mm^2 and ν=0.2, while the microstructure is based on mathematical modelling as discussed in section 2, with specific parameters for the three materials types. The sample cubes have side lengths of 6 mm for type A, 10 mm for type B and 12 mm for type C. Table 3 shows the re-calculated mean fracture strengths $\overline{\sigma}$ for the three types A – C, resulting from each 10 simulations per type. There are, of course, deviations from the experimentally determined values, but the qualitative tendency is well fitted.

Fig. 9 shows a refined stress-strain diagramm for a load process as in Fig. 7 with very small load increments. It looks more irregular than the curves in Fig. 4 and 7, even partial hardening happens. This effect is only of a geometrical-statistical nature, up to the load increment nothing in the model was changed.

6. Influence of microstructure on mean fracture strength

Using the procedure of section 5 the mean fracture strength $\overline{\sigma}$ was determined for some virtual, simulated samples of AAC, taking averages over 10 samples for each structure type.

6.1. Constant pore diameters

Three samples with pores of identical size were considered with pit radius $r_i \equiv 1$ mm and λ= 0.95. The artificial porosity had the values 15, 32 and 50%. Fig. 10 shows a planar section through

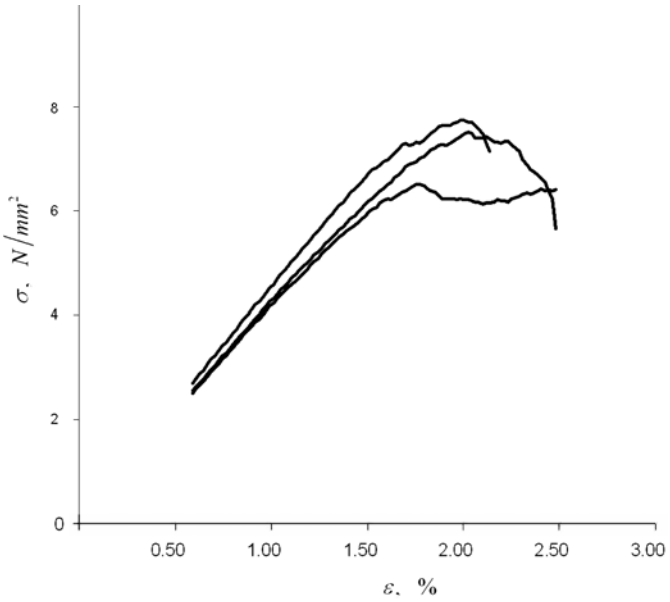

Fig. 9 Simulated stress-strain curves for a sample of type A with very small load increments

one of the virtual 15% samples in comparison to a planar section through a more irregular sample of type A, which has nearly the same porosity.

The corresponding mean fracture strengths $\overline{\sigma}$ were calculated as 4.20, 1.37 and 0.55 N/mm^2. As expected they are decreasing with increasing porosity. Comparison with the $\overline{\sigma}$-values in Table 3 shows that the mean fracture strengths for the virtual materials with constant pore radii are clearly smaller than those for more irregular materials of comparable porosities.

6.2. Bidisperse pore distribution

Now a series of virtual samples with more variability of pore sizes is considered. The pore diameter distribution is bidisperse, i.e., the diameters can take only two values d and D, with D=2 mm and d=1 mm. The samples differ in the percentage ρ of number of large pores, this ρ varies systematically between 0 and 100, where ρ=0% means only d-pores and ρ=100% only D-pores, i.e., monodisperse distribution. The porosity of all samples is the same (50%) and also the mechanical beam parameters are fixed, with the aim to model different types of AAC of the same material but different microstructure.

Fig. 11 shows the results, the mean fracture strength $\overline{\sigma}$ in dependence of the percentage ρ. Obviously, there is no great influence of ρ, the mean fracture strength ρ varies around 0.6 N/mm^2 for all samples. The maximum of mean fracture strength $\overline{\sigma}$ is obtained for ρ=40%, which corresponds to a mixture of 60% d-pores and 40% D-pores. Since the values of $\overline{\sigma}$ are nearly identical for ρ=0% and ρ=100%, there is obviously only a small size effect for samples in the order of the size of the samples considered. The sample with ρ=0% can be considered as another sample of the material with ρ=100%, with linear scaling factor 2.

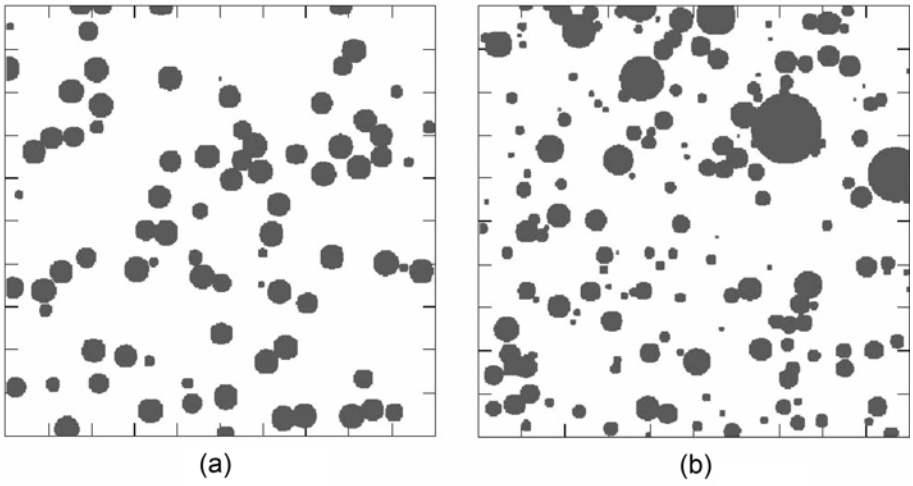

Fig. 10 Planar sections through samples of virtual AAC of artificial porosity 15%. Left: Constant pore diameter of 1 mm, right: variable pore diameters, following the model for type A

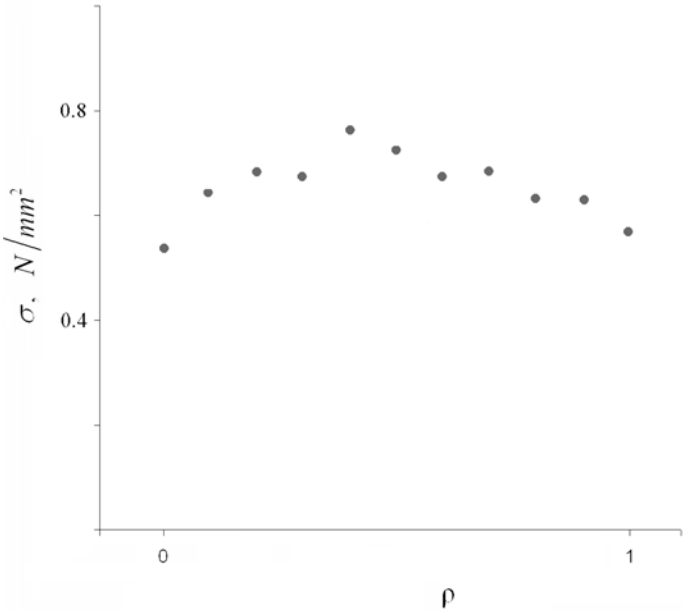

Fig. 11 Mean fracture strength of virtual AAC samples with bidisperse pore systems of diameters 1 and 2 mm in dependence on the percentage ρ of number of large pores

7. Conclusions

The paper presents an effective approach for the simulation of fracture processes in AAC. An approach is used which was already applied successfully for the prediction of Young moduli of such materials. It starts from the cherry-pit model for the system of pores. The radical tessellation based on the pits leads to an irregular geometrical network, the edges of which were used to construct a

beam network approximating the solid phase. The choice of these linear mechanical elements enables investigations for samples in the order of some mm. The mechanical properties of such networks are analyzed by standard FE methods. For the considered material AAC this approach is very successful, the relationship between mean fracture strength and microstructure can be investigated extensively. Still the sample sizes for simulated fracture tests are limited to dimensions of a few millimeters (side lengths of cubes). Thus a serious investigation of the size effect for large samples (such as used in industry) is not yet possible, which is for AAC not yet fully understood, see e.g., Wolf *et al*. (2005).

The reader should note that the frameworks used in the present paper are determined by the geometry of the porous medium. Therefore the standard question in FEM of effects of finer or coarser discretisation of the same microstructure does not make sense here.

It is expected that the approach described is applicable to other porous materials with pore systems that can be modeled by systems of hard spheres or cherry-pit models.

Acknowledgements

The authors are grateful to Dr. Luc Oger (Université Rennes, France) for the provided software for the calculation of radical tessellations. Financial support from the German Science Foundation (DFG) is gratefully acknowledged.

References

Bazant, Z.P. and Planas, J. (1997), *Fracture and Size Effect in Concrete and other Quasibrittle Materials*, CRC Press, Boca Raton, FL.

Bezrukov, A., Bargiel, M. and Stoyan, D. (2002), "Statistical analysis of simulated random packings of spheres", *Part. Part. Syst. Char.,* **19**, 111-118.

Böhm, H.J. (2004), *Mechanics of Microstructured Materials*, Springer, Wien.

Bolander, J.E. and Sukumar, N. (2005), "Irregular lattice model for quasistatic crack propagation", *Phys. Rev. B.,* **74**, 094106.

Christ, N.H., Friedberg, R. and Lee, T.D. (1982), "Random lattice field theory: general formulation", *Nucl. Phys. B.,* **210**, 337-346.

Garboczi, E.J. (1998), "Finite element and finite difference programs for computing the linear electric and elastic properties of digital images of random materials", *NIST Internal Report* 6269, Chapter 2.

Garboczi, E.J. and Day, A.R. (1995), "An algorithm for computing the effective linear elastic properties of heterogeneous materials: three-dimensional results for composites with equal Poisson ratios", *J. Mech. Phys., Solids,* **43**, 1349-1362.

Gervois, A., Oger, L., Richard, P. and Troadec, J.P. (2002), "Voronoi and radical tessellations of packings of spheres", *Computational Geometry and Applications (CGA'02)*, Amsterdam.

Gibson, L.J. and Ashby, M.F. (1997), *Cellular Solids: Structure and Properties*, Cambridge, University Press, Cambridge.

Hrenniko, A. (1941), "Solution of problems in elasticity by the framework method", *J. Appl. Mech. Tech. Phys.,* **12**, 169-175.

Illian, J., Penttinen, A., Stoyan, H. and Stoyan, D. (2008), *Statistical Analysis and Modelling of Spatial Point Patterns*, Chichester, J. Wiley and Sons.

Kadashevich, I. and Stoyan, D. (2008), "A beam-network model for autoclaved aerated concrete and its use for the investigation of relationships between Young's modulus and microstructure", *Comp. Mater. Sci.,* **43**, 293-300.

Kadashevich, I. and Stoyan, D. (2005), "Micro-mechanical effect analysis of AAC", in: Limbachiya, Roberts (Eds.), *Autoclaved Aerated Concrete*, Taylor & Francis Group, London, 219-228.

Kadashevich, I., Schneider, H.J. and Stoyan, D. (2005), "Statistical modeling of the geometrical structure of the system of artificial air pores in autoclaved aerated concrete", *Cement Concrete Res.,* **35**, 1495-1502.

Krajcinovic, D. (1996), *Damage Mechanics*, Amsterdam, North Holland.

Lachihab, A. and Sab, K. (2005), "Aggregate composites: a contact based modelling", *Comp. Mater. Sci.,* **33**, 467-490.

Lin, C. and Cohen, M.H. (1982), "Quantitative methods for microgeometric modeling", *J. Appl. Phys.,* **53**, 4152-4165.

Nishida, S. I. (2004), *Macro-and Microscopic Approach to Fracture*, WIT Press, Southampton.

Okabe, A., Boots, B., Sugihara, K. and Chiu, S. Nok (2000), *Spatial Tessellations, Concepts and Applications of Voronoi Diagrams, 2nd edition*., John Wiley & Sons, Chichester.

Pothuaud, L., Porion, P., Lespersailles, E., Benhamou, C.L. and Levitz, P. (2000), "A new method for three-dimensional skeleton graph analysis of porous media: application to trabecular bone microarchitecture", *J. Microsc.,* **199**, 149-161.

Richard, P., Oger, L., Troadec, J.P. and Gervois, A. (2001), "A model of binary assemblies of spheres", *Eur. Phys. J.E.* **6**, 295-303.

Roberts, A.P. and Garboczi, E.J. (2002), "Elastic properties of model random three-dimensional open-cell solids", *J. Mech. Phys. Solids,* **50**, 33-55.

Ryan, T.M. and van Rietbergen, B. (2005), "Mechanical significance of femoral head trabecular bone structure in Loris and Galago evaluated using micromechanical finite element methods", *Am. J. Phys. Anthropol.,* **126**, 82-96.

Sahimi, M. (2003), *Heterogeneous Materials II. Nonlinear and Break Down Properties and Atomistic Modeling*, Springer, New York.

Sahimi, M. and Arbabi, S. (1993), "Mechanics of disordered solids. I, Percolation on elastic networks with central forces", *Phys. Rev. B.,* **47**, 695-702.

Sahimi, M. and Arbabi, S. (1993), Mechanics of disordered solids. II. Percolation on elastic networks with bond-bending forces, *Phys. Rev. B.,* **47**, 703-712.

Stroeven, P. and Stroeven, M. (2001), "SPACE approach to concrete's space structure and its mechanical properties". *Heron,* **46**, 265-289.

Stroeven, M., Askes, H. and Sluys, L.J. (2004), "Numerical determination of representative volumes for granular materials". *Comput. Method. Appl. M.,* **193**, 3221-3238.

Telley, H., Liebling, T.M. and Mocellin, A. (1996), "The Laguerre model of grain growth in two dimensions I. Cellular structures viewed as dynamical Laguerre tessellations". *Philos. Mag.,* **73**, 395-408.

Torquato, S. (2002), *Random Heterogeneous Materials, Microstructure and Macroscopic Properties*, Springer, New York.

Wolf, S., Wiegand, S., Stoyan, D. and Walther, H. (2005), "The compressive strength of AAC - a statistical investigation", in: Limbachiya, Roberts (Eds.), *Autoclaved Aerated Concrete*, Taylor & Francis Group, London, 287-295.

NB